Journal of Metals, Materials and Minerals, 35(2), e2261, 2025

Graphitic carbon nitride loaded $Bi_4O_5I_2$ for elevated photocatalytic tetracycline degradation

Subhasish MISHRA[1], Barsha MARANDI[2], Kali SANJAY[2], and Rashmi ACHARYA[1,*]

[1] *Department of Chemistry, I.T.E.R., Siksha 'O' Anusandhan deemed to be University, Bhubaneswar, Odisha 751030, India*
[2] *Hydro & Electrometallurgy Division, CSIR-Institute of Mineral and Materials Technology(IMMT), Bhubaneswar 751013, Odisha, India*

***Corresponding author e-mail**: rashmiacharya@soa.ac.in, drrashmiacharya75@gmail.com

Received date:
23 December 2024
Revised date:
4 February 2025
Accepted date:
4 April 2025

Keywords:
$g\text{-}C_3N_4$;
$Bi_4O_5I_2$;
Heterojunction;
Z-Scheme;
Tetracycline

Abstract

As a robust photocatalyst, $Bi_4O_5I_2$ have has attracted significant scientific interest owing to its narrow bandgap energy, escalated electronic properties and high stability. Nonetheless, the unfavourable band structure and higher recombination of excitons have restricted its diversified photocatalytic applications. In this context, binary heterojunction construction using $Bi_4O_5I_2$ could be considered an effective strategy for spatial charge carrier separation across the hetero-interface, leading to an enhanced activity. In this study, we have prepared $Bi_4O_5I_2/g\text{-}C_3N_4$ Z-scheme hetero-structures via a wet impregnation strategy that preserves the spherical structure of $Bi_4O_5I_2$. The phase purity, chemical bonding, morphology and microstructure of the composite were confirmed using XRD, FTIR, SEM, TEM and HRTEM studies. The formation of robust 3D-2D contact junction triggers the charge separation and migration at the hetero-interface. Furthermore, the Z-scheme charge transfer dynamics helps to retain the redox ability of the excitons. As a result, The $Bi_4O_5I_2/g\text{-}C_3N_4$ heterojunction composite exhibited 84.6% of tetracycline degradation within 60 min that is 1.8 and 2.7 folds higher than pristine $Bi_4O_5I_2$ and $g\text{-}C_3N_4$, respectively. The findings of this study have major implications for building highly effective heterojunctions for upgraded photocatalytic applications.

1. Introduction

The rising presence of pharmaceutical pollutants in water bodies, such as tetracycline hydrochloride, has become a major environmental problem [1,2]. These persistent organic pollutants represent serious threats to aquatic ecosystems and human health [3]. To overcome this challenge, sophisticated water treatment technologies are urgently required. As a green and sustainable alternative, photocatalysis is emerging as a promising technique for pollutant degradation [4-7]. Recently many studies have focused on the efficient removal of organic contaminants from aqueous bodies using semiconductor mediated photocatalytic techniques. For instance, Li *et al.* have fabricated $Mn_{0.5}Cd_{0.5}S/Bi_2MoO_6$ S-scheme heterojunction photocatalyst for the effective removal of tetracycline drug molecules. The prepared catalyst exhibited superior tetracycline degradation efficiency with a rate constant of 0.0323 min^{-1} [8]. Similarly, Zhang group designed 0D/0D/1D core-shell S-scheme heterojunction containing carbon quantum dots, CdS and Ta_3N_5 for photocatalytic destruction of levofloxacin from waste water [9].

Bismuth oxyiodide ($Bi_4O_5I_2$) has received a lot of attention in photocatalytic applications thanks to of its unique electronic structure and high photocatalytic activity [10,11]. However, its practical application is frequently constrained by narrow light absorption window and elevated exciton recombination [12]. To address these constraints, a variety of techniques have been used, including the formation of heterojunctions with other semiconductors [13]. Construction of semiconductor-semiconductor heterojunction resulted in fast charge carrier separation through the heterointerface leading to significant decrease in charge recombination rate. Shen *et al.* demonstrated the enhanced degradation of tetracycline hydrochloride and levofloxacin in the presence of $Ag/Ag_6Si_2O_7/Bi_{12}O_{17}Cl_2$ S-scheme heterojunction. The formation of heterojunction and plasmon effect helped in the augmented separation of charge carriers that resulted in enhanced performance [14]. Similarly, number of research articles have demonstrated the benefits of heterojunctions for upgraded photocatalytic degradation of antibiotics [15,16].

Graphitic carbon nitride ($g\text{-}C_3N_4$) has emerged as a promising contender for heterojunction construction due to its favourable band structure, ability to absorb visible light, and superior chemical and thermal durability [17,18]. The staggered arrangement of band structures between $Bi_4O_5I_2$ and $g\text{-}C_3N_4$ established a robust heterojunction which supresses charge recombination effectively and promotes photocatalytic activity [19,20]. Zhang *et al.* have designed a $g\text{-}C_3N_4/Bi_4O_5I_2$ type–II heterojunction using a solvo-thermal technique for photocatalytic purification of eutrophic water [21]. The heterojunction construction helps in elevating the charge transfer and separation for upgraded photocatalytic performance. However, the type-II charge transfer scheme resulted in reducing the redox capability of the electrons and holes, which causes the material's inability to produce major reactive oxygen species such as $OH^{\bullet}$ and $O_2^{-\bullet}$ radicals that are essential for photocatalytic degradation process [22]. To tackle this, Z-Scheme charge transfer system should be considered. The Z-scheme mechanism reduces recombination by spatially separating the electron-hole pairs which permits them to take part in redox processes. Additionally, the redox ability of photoinduced charge carriers is enhanced since the available electrons belong to

more negative conduction band and the holes belong to more positive valence band [23]. Our group have previously described the synthesis of $Bi_4O_5I_2$/g-C_3N_4 Z-scheme based heterojunction using high temperature treatment method [24]. The resulted materials have also performed almost complete reduction of Cr(VI) and degradation of tetracycline synchronously with faster reaction kinetics. However, the interaction of g-C_3N_4 with the BiOI at high temperature causes distortion in the spherical morphology of $Bi_4O_5I_2$. This may lead to improper formation of 3D-2D heterojunction contact interface. Thus, a lower temperature wet chemical method would be considered which not only retains a robust 3D-2D $Bi_4O_5I_2$/g-C_3N_4 heterojunction but also keeps the spherical morphology of $Bi_4O_5I_2$ intact.

In this study, we have reported a wet chemical impregnation method to construct a $Bi_4O_5I_2$/g-C_3N_4 Z-Scheme heterojunction. The specific objectives of this research is to develop a facile and efficient method for the synthesis of g-C_3N_4-loaded $Bi_4O_5I_2$ composites with controlled morphology and composition with enhanced redox ability. The structural and morphological properties of the synthesized samples were obtained using various analytical techniques such as XRD, FTIR, SEM, TEM and HRTEM. The photocatalytic activity of the obtained materials was assessed by the degradation of tetracycline under solar light irradiation. Finally, the underlying photocatalytic mechanism of the was elucidated by employing radical trapping experiments. This study aims to promote sustainable water treatment technologies by offering insightful information on the design and development of effective photocatalysts for the degradation of organic contaminants.

2. Experimental

2.1 Chemicals

Thiourea (CH_4N_2S), ethanol (C_2H_5OH), tetracycline hydrochloride ($C_{22}H_{25}ClN_2O_8$) benzoquinone ($C_6H_4O_2$), isopropyl alcohol (C_3H_8O), triethanolamine ($C_6H_{15}NO_3$), diphenyl carbazide (DPC) and sulphuric acid (H_2SO_4) used in this work were of analytical grade from Merck Co., India

2.2 Graphitic carbon nitride (g-C_3N_4) fabrication

Pure g-C_3N_4 was prepared using simple thermal condensation method. Precisely, 10 g of thiourea was grinded for 1 h using mortar and pestle and subjected to thermal treatment inside a muffle furnace at 550°C for 4 h. The obtained yellowish powder was named as g-C_3N_4.

2.3 Preparation of $Bi_4O_5I_2$

$Bi_4O_5I_2$ microspheres were fabricated using a solvothermal assisted calcination method as reported earlier in our previous work [24].

2.4 Synthesis of $Bi_4O_5I_2$/gC_3N_4 composite

A wet impregnation method was followed to prepare $Bi_4O_5I_2$/g-C_3N_4 heterojunction. Briefly, 150 mg of the prepared g-C_3N_4 and 350 mg of $Bi_4O_5I_2$ were mixed with 25 mL ethanol. The solution was mixed properly using a magnetic stirrer at 60°C for 2 h to ensure the complete evaporation of ethanol. The dried yellow powder thus obtained was named as $Bi_4O_5I_2$/gC_3N_4 composite.

2.5 Instrumentation

Utilizing a Rigaku Miniflex X-Ray diffractometer (Japan) equipped with Cu Kα radiation (I = 1.54 Å, 40 kV, 100 mA), the structure and phase purity of the produced materials were evaluated. The samples' morphology was examined using a JEM-F-200 high resolution TEM and a Carl Zeiss Evo 18 SEM.

2.6 Photocatalytic performance assessment

The photocatalytic degradation of tetracycline was examined by exposing a 30 mg·L^{-1} of 50 mL tetracycline solution with 20 mg (0.4 g·L^{-1}) of produced photocatalyst for 1 h in direct sunlight. The tetracycline concentration in the aqueous solution was measured at 357 nm using the Systronic UV-visible spectrophotometer 2202. The percentage photocatalytic tetracycline degradation was calculated using the following expression.

$$\% \text{ Tetracycline degradation} = \frac{C_0 - C_t}{C_0} \times 100$$

Where C_0 is the initial tetracycline concentration and C_t stands for concentration of tetracycline at time t mins.

3. Results and discussions

3.1 Phase structure and morphology

The X-Ray diffraction technique has been used to evaluate the crystal structure and purity of the prepared samples. Pure $Bi_4O_5I_2$ displayed significant diffraction peaks at 28.81°, 31.3°, 37.28°, 44.92°, 49.4° and 54.3° representing (41–1), (402), (–404), (422), (006) and (811) planes of pure phase $Bi_4O_5I_2$ (ICSD #412590) [25]. Similarly the two characteristic diffraction peaks for g-C_3N_4 located at 13.2° and 27.4° are related to the C-N heterocycles and inter-layer stacking of the nanosheets, respectively (JCPDS #87-1526) [26]. The as-prepared $Bi_4O_5I_2$/g-C_3N_4 composite shows all the peaks present in $Bi_4O_5I_2$ phase. However it doesn't displayed any peaks associated to g-C_3N_4 due to the presence of less amount of g-C_3N_4 in the composite.

Interestingly after the composite formation, the peak corresponding to (41–1) plane of $Bi_4O_5I_2$ gets broader and less intense. This suggested interaction between both the materials [27]. Furthermore, the absence of any unidentified peak in the XRD patterns indicated the absence of any foreign materials and pure phase formation. The chemical states of the molecules in the fabricated catalysts has been accessed using Fourier Transformed Infra-Red (FTIR) spectroscopy (Figure 2(b)). The pure g-C_3N_4 exhibited its most prominent peak at around 810 cm^{-1} corresponding to the breathing mode of triazine units. The group of peaks from 1200 cm^{-1} to 1700 cm^{-1} signifies the stretching vibration of the C-N heterocycles [28]. For pure $Bi_4O_5I_2$, the identified peak positioned at 490 cm^{-1} suggested the stretching mode of Bi-O bonding [29]. In the FTIR spectra of $Bi_4O_5I_2$/g-C_3N_4 heterojunction,

the presence of the peaks corresponding to breathing mode of triazine units at 813 cm^{-1} and stretching mode of Bi-O bonds at 492 cm^{-1} confirms the presence of both g-C_3N_4 and $Bi_4O_5I_2$ in the composite. Additionally, the intensity of the cluster of peaks around 1200 cm^{-1} to 1700 cm^{-1} was decreased in the composite as compared to pristine g-C_3N_4 suggesting a close interaction at the hetero-interface.

The morphology of the obtained samples were studied using SEM technique. Pristine $Bi_4O_5I_2$ displayed a regular spherical structure (Figure 2(a)) with average diameter ranging from 0.43 µM to 3.5 µM. These $Bi_4O_5I_2$ microspheres are properly spherical in shape as well as arranged homogenously. The pristine g-C_3N_4 displayed rough and porous arrangement of stacked layers (Figure 2(b)). The release of gases like NH_3 and CO_2 due to high temperature treatment resulted in the formation of wrinkles and rough surfaces in g-C_3N_4 [30]. Figure 2(c) displayed the TEM image of $Bi_4O_5I_2$/g-C_3N_4 composite. The black spheres represented the $Bi_4O_5I_2$ and g-C_3N_4 was identified as transparent sheets. This suggested that fabrication through wet impregnation technique retained the spherical morphology of $Bi_4O_5I_2$ in the composite with the formation of robust 3D-2D $Bi_4O_5I_2$/g-C_3N_4 heterojunction. To confirm the formation of heterojunction between $Bi_4O_5I_2$ and g-C_3N_4, HRTEM analysis was performed. The lattice patterns illustrated in Figure 2(d) displayed two types of d-spacing values. The fringes with a d-spacing value of 0.33 represented (002) plane of g-C_3N_4 while that with 0.31 nm corresponds to (41–1) plane of $Bi_4O_5I_2$ [31]. The coexistence of these fringe patterns confirmed the formation of heterojunction with proper interfacial interaction.

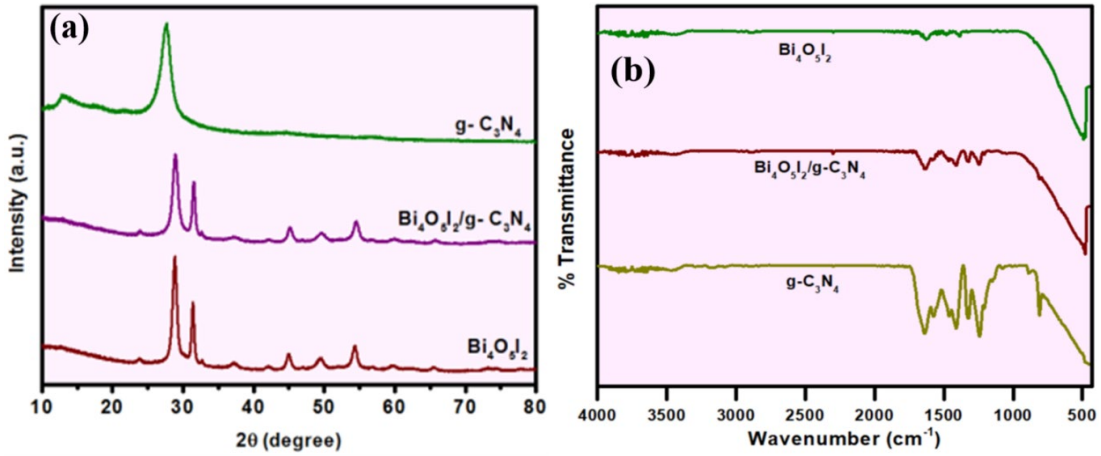

Figure 1. (a) X-Ray diffraction patterns, and (b) FTIR spectra of g-C_3N_4, $Bi_4O_5I_2$, and $Bi_4O_5I_2$/g-C_3N_4 composite.

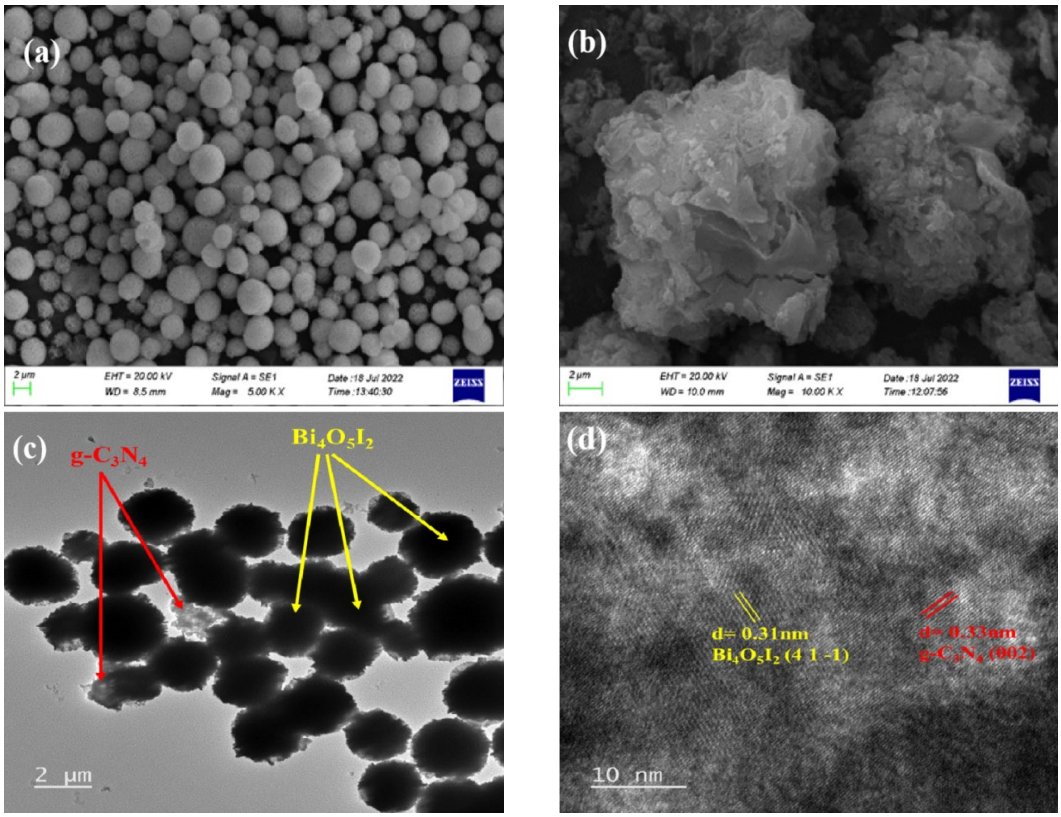

Figure 2. SEM images of (a) $Bi_4O_5I_2$ and (b) g-C_3N_4, (c) TEM and (d) HRTEM images with lattice patterns of $Bi_4O_5I_2$/g-C_3N_4 heterojunction.

3.2 Photocatalytic tetracycline degradation activity

The photocatalytic performance of the prepared materials have been examined by using tetracycline as a targeted pollutant under visible light irradiation. First of all, dark absorption experiments were carried out for 30 min to establish adsorption-desorption equilibrium between the catalyst and the pollutant molecules. To evaluate the degree of TCH adsorption on the photocatalyst, sorption experiments were conducted in dark conditions. Figure 3(a) illustrates the adsorption efficiency of the synthesized samples for TCH uptake. After 60 min, $Bi_4O_5I_2$/g-C_3N_4 heterojunction demonstrated the highest adsorption efficiency, reaching approximately 8% for TCH. The adsorption curves exhibited a decline over time, stabilizing at around 30 min. Consequently, an adsorption-desorption equilibrium between the catalyst and pollutant molecules was achieved within 30 min.

The pollutant solution containing catalysts was then exposed to direct sunlight for 1 h with magnetic stirring to carryout phtocatalytic degradation reactions of tetracycline. Figure 3(b) illustrated that the $Bi_4O_5I_2$/g-C_3N_4 composite exhibited maximum activity by eliminating 84.6% of tetracycline followed by pristine $Bi_4O_5I_2$ (47.2%) and g-C_3N_4 (31.3%). This enhanced photocatalytic activity could be ascribed to the construction of a strong heterojunction between $Bi_4O_5I_2$ and g-C_3N_4, which augmented the charge separation and migration across the hetero-interface. This results in reduced exciton recombination and upgraded photocatalytic performance. The photocatalytic degradation kinetics was studies using Langmuir–Hinshelwood kinetic model [32].

The linearly fitted curves present in Figure 3(c) demonstrated the pseudo first order reaction kinetics was followed in the degradation process. The derived reaction rate constant (k) values were 0.037 min^{-1}, 0.014 min^{-1} and 0.005 min^{-1} for $Bi_4O_5I_2$/g-C_3N_4. $Bi_4O_5I_2$ and g-C_3N_4 respectively. Higher rate constant also suggest that the photocatalytic oxidation takes place faster in case of the composite due to lower recombination. Table 1 illustrates the comparison of tetracycline degradation efficiency of the prepared materials with different Bi-based systems.

The pH of the pollutant solution can greatly affect the surface charge of the catalyst as well as the production of oxygen species that leads to higher photocatalytic activity. The effect of pH of the TCH solution on the photocatalytic degradation has been investigated at different pH (i.e. 3, 5, 7, 9, 11). Figure 3(d) shows the % tetracycline degradation by the $Bi_4O_5I_2$/g-C_3N_4 composite catalyst at different pH. According to the figure, the change in the pH of the solution does not have a significant effect on the degradation process. Notably, in acidic conditions, the photocatalytic activity is relatively higher. This might be due to the fact that $OH^{\bullet}$ radicals predominates at higher pH while h^+ ions are the dominating species in acidic medium. Since the catalyst surface is negatively charged, the h^+ ions get attracted towards the catalyst suitably rather than $OH^{\bullet}$ radicals. This leads to higher activity at lower pH [40].

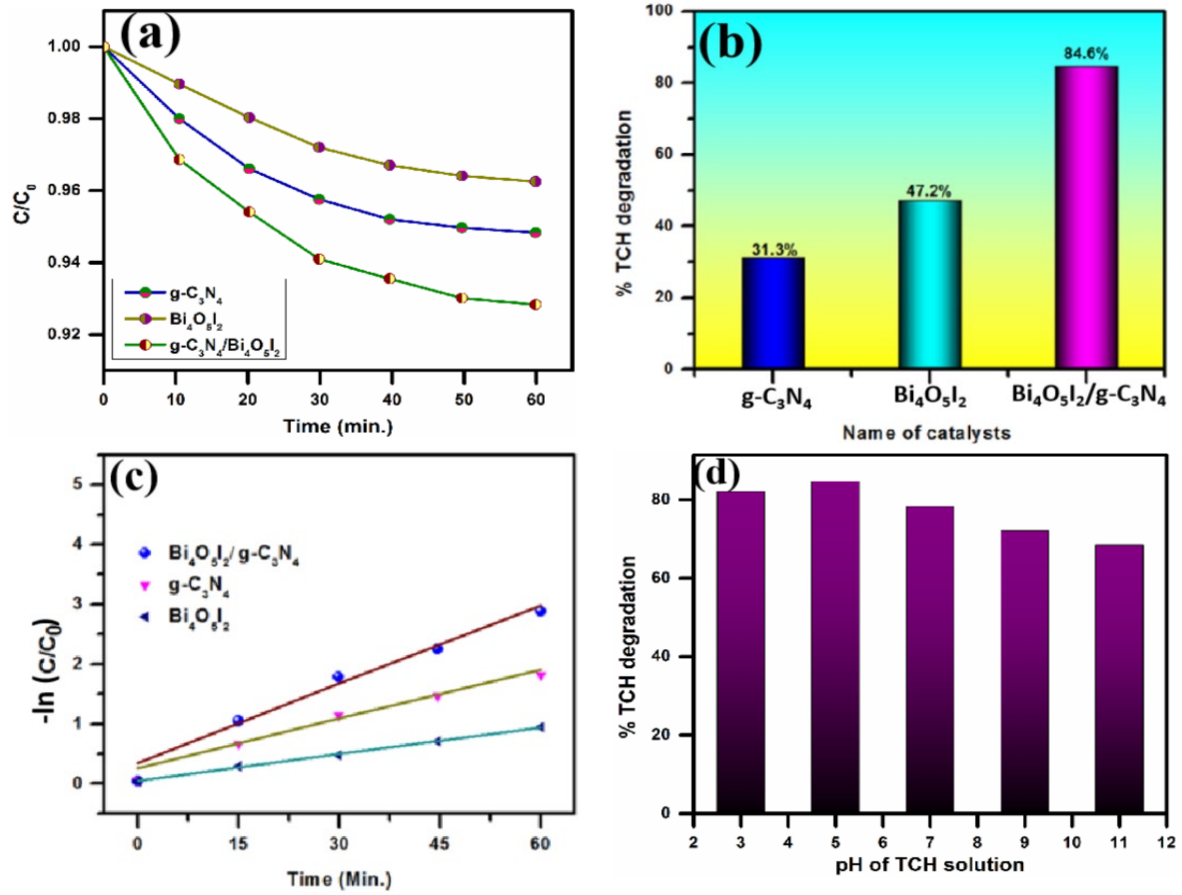

Figure 3. (a) TCH adsorption ability of the prepared catalysts in dark, (b) photocatalytic tetracycline degradation performance, (c) linearly fitted reaction kinetics curves for the prepared materials, (d) effect of solution pH on the photocatalytic TCH degradation efficiency (TCH concentration = 30 mg·L^{-1}, catalyst dose = 0.4 g·L^{-1}, pH = 5, intensity = 100000 lux for 60 min).

Table 1. Comparison of tetracycline degradation efficiency and rate constant value of the prepared catalysts with that of Bi-based photocatalytic systems.

Catalyst	Dose [g·L^{-1}]	TCH concentration	Time [min]	Light source	% TCH degradation	Rate constant k [min^{-1}]	Ref.
AgBr/Bi_2WO_6 Z-scheme	1	20 mol·L^{-1}	60	Xe lamp	87.5	0.02	33
g-C_3N_4/$NaBiO_3$ Z-scheme	1	25 ppm	30	Xe lamp	87.1	0.073	34
Bi_2O_4/g-C_3N_4	0.5	20 ppm	60	Xe lamp	97.5	0.056	35
Bi_2WO_6/g-C_3N_4 Z-scheme	0.4	20 ppm	60	Direct sunlight	98	0.044	36
g-C_3N_4/Bi_5O_7I Z-scheme	0.7	10 ppm	180	Visible light	98.7	0.015	37
g-C_3N_4/Na-$BiVO_4$	0.2	20 ppm	40	Xe lamp	78.9	0.109	38
TiO_2/BiOCl Z-scheme	0.5	20 ppm	60	Visible light	~82	0.03	39
BiOI/g-C_3N_4 Z-scheme	1	20 ppm	30	Xe lamp	86	0.07	40
$Bi_4O_5I_2$/g-C_3N_4 Z-scheme	0.4	30 ppm	60	Direct sunlight	84.6	0.037	This work

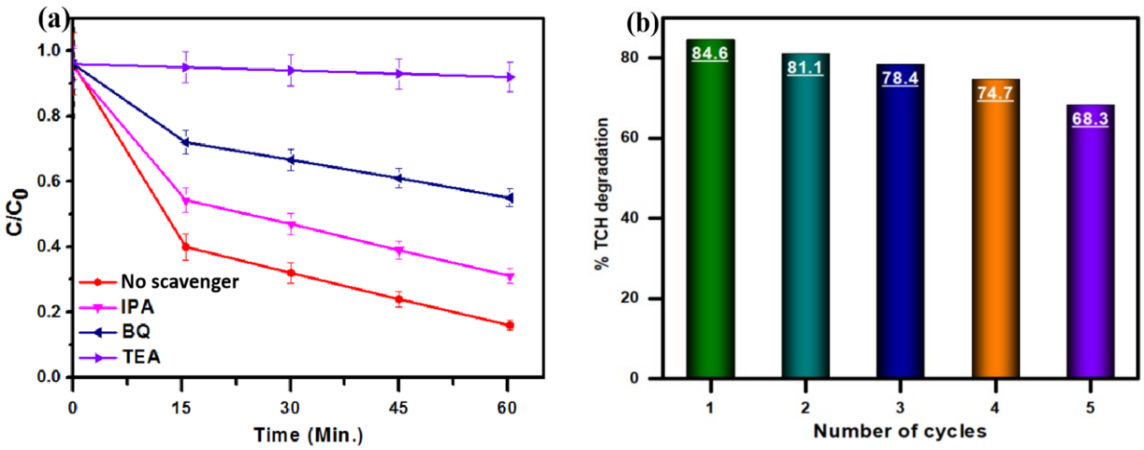

Figure 4. (a) Radical trapping experiment results of tetracycline photocatalytic degradation, and (b) recycle experiments for TCH degradation over composite

3.3 Photocatalytic reaction mechanism

Scavenging tests were used to examine the photocatalytic mechanism involved in tetracycline breakdown. The roles of major reactive species such as holes (h^+), superoxide ions ($O_2^{-\bullet}$) and hydroxyl radicals ($OH^\bullet$) in photocatalytic degradation was assessed by quenching them with triethanolamine (TEA), p-benzoquinone (BQ), and Isopropanol (IPA), respectively as sacrificial agents. Figure 4(a) depicts the tetracycline degradation rate in the presence of applied scavengers. The figure clearly illustrates that the produced catalyst degrades tetracycline to the greatest extent when exposed to IPA. This indicates that $OH^\bullet$ radicals play a secondary role in the degradation process. When TEA is used as a scavenger, catalytic activity is reduced to a minimum, identifying holes as the principal reactive species. This study showed that the photocatalytic breakdown process is predominantly dominated by the h^+, $O_2^{-\bullet}$ and $OH^\bullet$ species.

The prevalence of holes and superoxide radicals as the major reactive species suggests the formation of Z-Scheme heterojunction between $Bi_4O_5I_2$ and g-C_3N_4 rather than a type-II heterojunction. In case of a type-II mechanism, the electrons and holes would gather at the CB of $Bi_4O_5I_2$ and VB of g-C_3N_4 after the irradiation of solar light. This restricts the formation of both $O_2^{-\bullet}$ and $OH^\bullet$ radicals owing to unfavourable band potentials. However, our study shows the generation of both of these radicals as the major reactive oxygen species in degradation process. This can only be possible if a direct Z-scheme charge transfer is considered. The underlying photocatalytic mechanisms can be explained as follows:

When the composite catalyst is exposed to solar radiation, the electrons present in the VB of both g-C_3N_4 and $Bi_4O_5I_2$ gets excited towards their respective CBs. As per the Z-scheme charge transfer system, the electrons present in the CB of $Bi_4O_5I_2$ migrate towards the VB of g-C_3N_4. The holes in the VB of g-C_3N_4 and electrons in the CB of $Bi_4O_5I_2$ gets recombine due to the staggered arrangement and band bending at the semiconductor interface. Lastly, the electrons present in the CB of g-C_3N_4 and holes in the VB of $Bi_4O_5I_2$ with high redox potentials gets preserved at their respective positions. This separation of charge carriers with higher activity results in the formation of superoxide radicals and holes which play major roles in the photocatalytic degradation of tetracycline. Scheme 1 represents the photocatalytic degradation mechanism of tetracycline in aqueous medium using $Bi_4O_5I_2$/g-C_3N_4 heterojunction as a catalyst.

The stability of the photocatalyst is an important aspect to upscale its practical applications. The as-prepared $Bi_4O_5I_2$/g-C_3N_4 photocatalyst has been tested repeatedly for five cycles of photocatalytic tetracycline degradation and the results has been illustrated in Figure 4(b). The composite exhibited high TCH degradation efficiency for four consecutive cycles without significant loss in the activity. However, $Bi_4O_5I_2$/g-C_3N_4 showed decrease in the activity after the fourth cycle. This might be ascribed to the loss of active sites present over the catalyst surface.

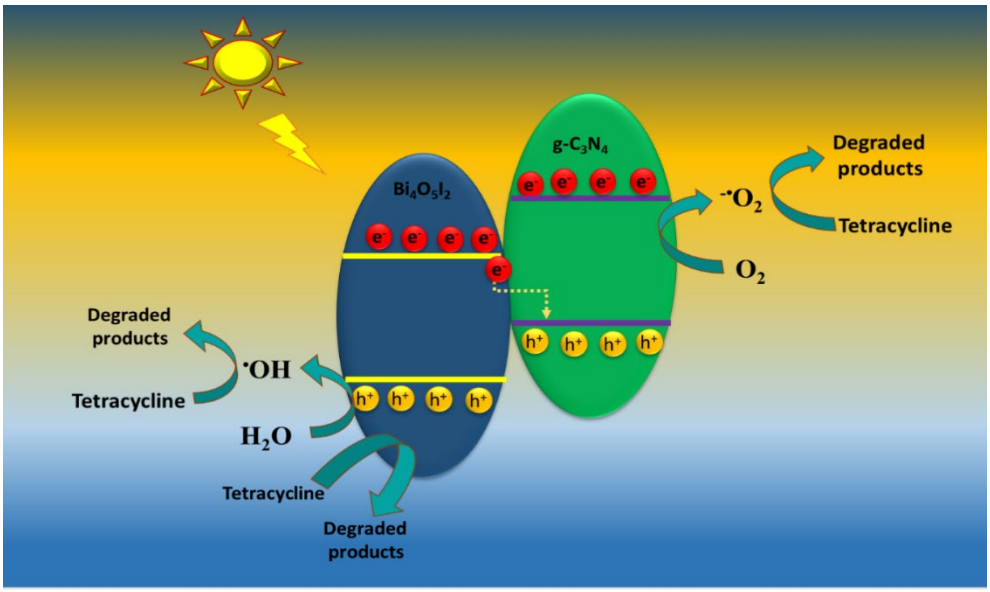

Scheme 1. Photocatalytic degradation mechanism of tetracycline in aqueous medium using $Bi_4O_5I_2$/g-C_3N_4 heterojunction as a catalyst.

4. Conclusions

To conclude, we have fabricated $Bi_4O_5I_2$/g-C_3N_4 Z-Scheme heterojunction using a wet impregnation method for improved degradation of tetracycline. The use of wet chemical method for the fabrication of heterojunction preserves the spherical structure of $Bi_4O_5I_2$. This ensures proper contact interface between $Bi_4O_5I_2$ microspheres and g-C_3N_4 nanosheets to obtain 3D-2D morphology based heterojunction. The phase purity, chemical structure, morphology and microstructure of the prepared material were investigated using XRD, FTIR, SEM and TEM analysis. The formation of heterojunction was confirmed from the lattice fringes observed in HRTEM image. The photocatalytic performance of the prepared catalysts was examined using TCH drug under direct sunlight. The fabricated $Bi_4O_5I_2$/g-C_3N_4 heterojunction exhibited 84.6% of tetracycline degradation within 1 h which is 1.8 time and 2.7 time greater than pure $Bi_4O_5I_2$ and g-C_3N_4, respectively. The boosted charge separation and the diminished exciton recombination are responsible for this upgraded performance. From the radical trapping experiments, h^+, $O_2^{-\bullet}$ and $OH^\bullet$ radicals are confirmed to be major reactive species. Formation of a Z-Scheme charge transfer system preserves the redox potential of charge carriers and reduces recombination as well. We hope this work would give new ideas to synthesize Z-Scheme heterojunctions with robust contact interface for aquatic pollutant degradation.

Acknowledgment

The authors extend their sincere thanks to the management of Siksha "O" Anusandhan (Deemed to be University), Bhubaneswar, Odisha, India, for constant support and assistance in finishing this work.

References

[1] M. H. Firooz, A. Naderi, M. Moradi, and R. R. Kalantary, "Enhanced tetracycline degradation with TiO_2/natural pyrite S-scheme photocatalyst," *Scientific Reports*, vol. 14, no. 4954, 2024.

[2] Z. Hu, Y. Wang, L. Wang, Q. Wang, Q. Zhang, F. Cui, and G. Jiang, "Synthesis of S-type heterostructure π-COF for photocatalytic tetracycline degradation," *Chemical Engineering Journal*, vol. 479, p. 147534, 2024.

[3] L. Yang, Y. Liu, P. Tan, Y. Lu, Q. Ding, and J. Pan, "Anchoring TiO_2@$CsPbBr_3$ on g-C_3N_4 nanosheet for enhanced photocatalytic degradation activity of tetracycline hydrochloride," *Diamond and Related Materials*, vol.133, p. 109727, 2023.

[4] K. khoirunisa, N. D. lestari, E. T. wahyuni, and T. A. natsir, "Enhanced photocatalytic reduction of Cr(VI) under visible light a magnetically separable TiO_2-Fe/Fe_3O_4 photocatalyst prepared from iron rusty waste", *Journal of Metals, Materials and Minerals*, vol. 35, no. 1, p. e2162, 2025.

[5] S. Mishra, and R. Acharya, "Recent updates in modification strategies for escalated performance of graphene/MFe_2O_4 heterostructured photocatalysts towards energy and environmental applications," *Journal of Alloys and Compounds*, vol. 960, p.170576, 2023.

[6] R. Acharya, S. Mishra, and A. Naik, "Development of graphene-based photocatalysts for remediation of hexavalent chromium," In: M.R. Johan, M.N. Naseer, M. Ikram, A. A Zaidi, Y. Abdul Wahab, (eds) Graphene-Based Photocatalysts. Advanced Structured Materials, vol 217, pp. 317-345, Springer 2024.

[7] S. Mishra, R. Acharya, and K. Parida, "Spinel-ferrite-decorated graphene-based nanocomposites for enhanced photocatalytic detoxification of organic dyes in aqueous medium: a review," *Water,* vol. 15, p. 81, 2023.

[8] S. Li, C. You, F. Yang, G. Liang, C. Zhuang, and X. Li, "Interfacial Mo–S bond modulated S-scheme $Mn_{0.5}Cd_{0.5}S$/Bi_2MoO_6 heterojunction for boosted photocatalytic removal of emerging organic contaminants," *Chinese Journal of Catalysis,* vol. 68, p. 259, 2025.

[9] S. Li, K. Rong, X. Wang, C. Shen, F. Yang, and Q. Zhang, "Design

of carbon quantum dots/CdS/Ta_3N_5 S-Scheme heterojunction nanofibers for efficient photocatalytic antibiotic removal, *Acta Physico-Chimica Sinica*, vol. 40, p. 2403005, 2024.

[10] F. Chang, H. Chen, X. Zhang, B. Lei, and X. Hu, "n-p heterojunction $Bi_4O_5I_2/Fe_3O_4$ composites with efficiently magnetic recyclability and enhanced visible-lightdriven photocatalytic performance," *Separation and Purification Technology*, vol. 238, p. 116442, 2020.

[11] H. Zhang, X. Zhang, Z. Zhang, X. Ma, Y. Zhu, and M. Ren, Y. Cao, and P. Yang, "Ultrahigh charge separation achieved by selective growth of $Bi_4O_5I_2$ nanoplates on electron accumulating facets of Bi_5O_7I nanobelts," *ACS Applied Materials and Interfaces*, vol. 13, pp. 39985-40001, 2021.

[12] M. Ji, J. Di, Y. Liu, R. Chen, K. Li, Z. Chen, J. Xia, and H. Li, "Confined active species and effective charge separation in $Bi_4O_5I_2$ ultrathin hollow nanotube with increased photocatalytic activity," *Applied Catalysis B: Environmental*, vol. 268, p. 118403, 2020.

[13] Z. Shen, H. Liu, X. Jia, Q. Han, and H. Bi, "Phase transformation and heterojunction construction of bismuth oxyiodides by grinding-assisted calcination in the presence of thiourea and their photoactivity," *Dalton Transitions*, vol. 50, p. 7464-7473, 2021.

[14] C. Shen, X. Li, B. Xue, D. Feng, Y. Liu, F. Yang, M. Zhang, and S. Li, "Surface plasmon effect combined with S-scheme charge migration in flower-like $Ag/Ag_6Si_2O_7/Bi_{12}O_{17}Cl_2$ enables efficient photocatalytic antibiotic degradation," *Applied Surface Science,* vol. 679, p. 161303, 2025.

[15] S. Li, R. Yan, M. Cai, W. Jiang, M. Zhang, and X. Li, "Enhanced antibiotic degradation performance of $Cd_{0.5}Zn_{0.5}S/Bi_2MoO_6$ S-scheme photocatalyst by carbon dot modification," *Journal of Materials Science & Technology,* vol. 164, p. 59, 2023.

[16] C. Wang, K. Rong, Y. Liu, F. Yang, and S. Li, "Carbon quantum dots-modified tetra (4-carboxyphenyl) porphyrin/BiOBr S-scheme heterojunction for efficient photocatalytic antibiotic degradation." *Science China Materials,* vol. 67, p. 562, 2024.

[17] R. Acharya, S. Pati, and K. Parida, "A review on visible light driven spinel ferrite-g-C_3N_4 photocatalytic systems with enhanced solar light utilization," *Journal of Molecular Liquids,* vol. 357, p. 119105, 2022.

[18] R. Acharya, S. Mishra, L. Acharya, and K. Parida, "Graphitic carbon nitride (g-C_3N_4)-based photocatalysts for environmental applications," In: N. Kumar, R. Gusain, Sinha S. Ray (eds) *Two-Dimensional Materials for Environmental Applications*. Springer Series in Materials Science, vol 332, p. 103, Springer 2023.

[19] J. Xia, M. Ji, J. Di, B. Wang, S. Yin, Q. Zhang, M. He, and H. Li, "Construction of ultrathin $C_3N_4/Bi_4O_5I_2$ layered nanojunctions via ionic liquid with enhanced photocatalytic performance and mechanism insight." *Applied Catalysis B: Environmental*, vol. 191, p. 235, 2016.

[20] Z. Feng, L. Zeng, Q. Zhang, S. Ge1, X. Zha, H. Lin, and Y. He, "In situ preparation of g-$C_3N_4/Bi_4O_5I_2$ complex and its elevated photoactivity in Methyl Orange degradation under visible light" *Journal of Environmental Sciences*, vol. 87, p. 149-162, 2020.

[21] Q. Zhang, L. Wang, H. Peng, S. Jiang, X. Xu , J. Xu, and K. Xu, "Construction of g-$C_3N_4/Bi_4O_5I_2$ heterojunction via the solvothermal method for the purification of eutrophic water," *Catalysis Communications*, vol. 149 p. 106200, 2021.

[22] J. Low, C. Jiang, B. Cheng, S. Wageh, A. A. Al-Ghamdi, J. Yu, "A review of direct Z-Scheme photocatalysts," *small*, vol. 1, p. 1700080, 2017.

[23] Y. Wang, Y. Ma, L. Chu, and X. LI, "In-situ embedding of nanocylindrical $Bi_{25}FeO_{40}$ into scaffold-C_3N_4 for enhanced Z-scheme photocatalytic degradation", *Journal of Metals, Materials and Minerals*, vol. 34, no. 4, p. 2167, 2024.

[24] S. Mishra, L. Acharya, B. Marandi, K. Sanjay, and R. Acharya, "Boosted photocatalytic accomplishment of 3D/2D hierarchical structured $Bi_4O_5I_2$/g-C_3N_4 p-n type direct Z-scheme heterojunction towards synchronous elimination of Cr(VI) and tetracycline," *Diamond and Related Materials*, vol. 142, p 110834, 2024.

[25] R. Yin, Y. Li, K. Zhong, H. Yao, Y. Zhang, and K. Lai, "Multifunctional property exploration: $Bi_4O_5I_2$ with high visible light photocatalytic performance and a large nonlinear optical effect," *RSC Advances*, vol. 9, p. 4539, 2019.

[26] X. Chen, R. Shi, Q. Chen, Z. Zhang, W. Jiang, W. Zhu, and T. Zhang, "Three-dimensional porous g-C_3N_4 for highly efficient photocatalytic overall water splitting," *Nano Energy*, vol. 59, pp. 644-650, 2019.

[27] J. He, J. Hu, Y. Hu, S. Guo, Q. Huang, Y. Li, G. Zhou, T. Gui, N. Hu, X. Chen, "Hierarchical S-scheme heterostructure of $CdIn_2S_4$@UiO-66-NH_2 toward synchronously boosting photocatalytic removal of Cr(VI) and tetracycline," *Inorganic Chemistry,* vol. 61, p. 19961-19973, 2022.

[28] X. Chen, R. Shi, Q. Chen, Z. Zhang, W. Jiang, W. Zhu, and T. Zhang, "Three-dimensional porous g-C_3N_4 for highly efficient photocatalytic overall water splitting," *Nano Energy,* vol. 59, p. 644, 2019.

[29] O. Mehraj, B.M. Pirzada, N.A. Mir, M.Z. Khan, and S. Sabir, "A highly efficient visible light-driven novel p-n junction Fe_2O_3/BiOI photocatalyst: surface decoration of BiOI nanosheets with Fe_2O_3 nanoparticles," *Applied Surface Science,* vol. 387, p.642, 2016.

[30] W. Zhang, H. He, H. Li, L. Duan, L. Zu, Y. Zhai, W. Li, L. Wang, H. Fu, and D. Zhao, "Visible-light responsive TiO_2-based materials for efficient solar energy utilization," *Advanced Energy Materials*, vol. 11, p. 2003303, 2021.

[31] H. Zhang, S. Tan, D. Wang, J. Wu, W. Xu, S. Zhao, X. Sun, Q. Liu, H. Liu, and Y. Guan, "Fabrication of bionic flower-like g-$C_3N_4/Bi_4O_5I_2$ photocatalyst with enhanced photocatalytic performance," *Chemical Physics Letters*, vol. 751, p. 137533, 2020.

[32] S. Mishra, L. Acharya, S. Sharmila, K. Sanjay, and R. Acharya, "Designing g-$C_3N_4/NiFe_2O_4$ S-scheme heterojunctions for efficient photocatalytic degradation of Rhodamine B and tetracycline hydrochloride," *Applied Surface Science Advances*, vol. 24, p. 100647, 2024.

[33] D. Huang, J. Li, G. Zeng, W. Xue, S. Chen, Z. Li, R. Deng, Y. Yang, and M. Cheng, "Facile construction of hierarchical flower-like Z-scheme $AgBr/Bi_2WO_6$ photocatalysts for effective

removal of tetracycline: Degradation pathways and mechanism," *Chemical Engineering Journal* , *vol. 375,* p. 121991*,* 2019.

[34] Y. Wu, X. Zhao, S. Huang, Y. Li, X. Zhang, G. Zeng, L. Niu, Y. Ling, and Y. Zhang, "Facile construction of 2D g-C_3N_4 supported nanoflower-like $NaBiO_3$ with direct Z-scheme heterojunctions and insight into its photocatalytic degradation of tetracycline," *Journal of Hazardous Materials* vol. 414, p.125547, 2021.

[35] J. Yang, Z. Liu, Y. Wang, and X. Tang, "Construction of the rod-like Bi_2O_4 modificated porous g-C_3N_4 nanosheets heterojunction of photocatalysts for the degradation of tetracycline," *New Journal of Chemistry,* vol. 44, p. 9725, 2020.

[36] Y. Li, H. Zhang, D. Zhang, S. Yao, S. Dong, Q. Chen, F. Fan, H. Jia, and M. Dong, "Construction of Bi_2WO_6/g-C_3N_4 Z-scheme heterojunction and its enhanced photocatalytic degradation of tetracycline with persulfate under solar light," *Molecules*, vol. 29, p. 1169, 2024.

[37] D. Tan, F. Huang, S. Guo, D. Li, Y. Yan, and W. Zhang, "Efficient photocatalytic tetracycline elimination over Z-scheme g-C_3N_4/Bi_5O_7I heterojunction under sunshine light: Performance, mechanism, DFT calculation and pathway," *Journal of Alloys and Compounds,* vol. 946, p. 169468, 2023.

[38] J. Kang, Y. Tang, M. Wang, C. Jin, J. Liu, S. Li, Z. Li, J. Zhu, "The enhanced peroxymonosulfate-assisted photocatalytic degradation of tetracycline under visible light by g-C_3N_4/$NaBiVO_4$ heterojunction catalyst and its mechanism" *Journal of Environmental Chemical Engineering,* vol. 9, p.105524, 2021.

[39] X. Zou, C. Li, L. Wang, W. Wang, J. Bian, H. Bai, and X. Meng, "Enhanced visible-light photocatalytic degradation of tetracycline antibiotic by 0D/2D TiO_2(B)/BiOCl Z-scheme heterojunction: Performance, reaction pathways, and mechanism investigation," *Applied Surface Science,* vol. 630, p. 157532, 2023.

[40] H. Liu, W. Huo, T. C. Zhang, L. Ouyang, and S. Yuan, "Photo-catalytic removal of tetracycline by a Z-scheme heterojunction of bismuth oxyiodide/exfoliated g-C_3N_4: performance, mechanism, and degradation pathway," *Materials Today Chemistry,* vol. 23, p. 100729, 2022.